High frequency phased array ultrasonic testing of thermoplastic tensile specimens manufactured by fused filament fabrication with embedded defects

K. Fayazbakhsh[1*], F. Honarvar[2], H. Amini[3], and A. Varvani-Farahani[4]

[1]Department of Aerospace Engineering, Ryerson University, 350 Victoria Street, Toronto, Ontario M5B2K3, Canada
[2]K. N. Toosi University of Technology, Faculty of Mechanical Engineering, 7 Pardis Street, Mollasadra Avenue, Vanak Square, Tehran, Iran
[3]FUJIFILM VisualSonics, Inc., 3080 Yonge Street, Suite 6100, Box 66, Toronto, ON, Canada, M4N 3N1, Canada
[4]Department of Mechanical and Industrial Engineering, Ryerson University, 350 Victoria Street, Toronto, ON, M5B 2K3, Canada
[*]Corresponding author: kazem@ryerson.ca; Tel: (+1) 416-979-5000 ext. 6414; fax: (+1) 416-979-5056; https://orcid.org/0000-0003-3963-8282

Abstract

Fused filament fabrication (FFF) is a popular additive manufacturing process used for fabrication of polymeric components. In this paper, defects are intentionally designed and induced in FFF 3D printed tensile specimens made from polylactic acid (PLA) per ASTM D638-14. Each fabricated sample consists of 24 layers and has a quasi-isotropic layup of $[45/0/90/-45]_{3s}$. The defects (gaps) are in the form of 5, 7, 9 and 11 adjacent missing extrudates in the 10^{th} layer, which has a 0° raster angle. Five specimens per each gap width, including no gap as the baseline, are 3D printed for a total of 25 specimens. The specimens are first scanned by high-frequency phased array ultrasonic testing (PAUT) and their layups are then accurately captured. This is the first time such high-resolution images are prepared from individual layers of 3D printed parts fabricated by FFF process. The as-manufactured gap widths are found to be within 10% of the as-designed values and are generally smaller. Next, the specimens are subjected to destructive tensile testing and their tensile properties are compared to the baseline. The relationship between the gap width and tensile properties of the specimens supports the suitability of high frequency PAUT for non-destructive testing of 3D printed parts.

Keywords: Phased array; Ultrasonic testing; Fused filament fabrication; Tensile testing; Gaps

Additive Manufacturing Journal

https://doi.org/10.1016/j.addma.2021.102335

1. Introduction

Additive manufacturing (AM) process has been categorized into seven major processes [1]; one of which is material extrusion (MEX), also known as Fused Filament Fabrication (FFF). In this processing technique, molten material is selectively deposited in a pre-determined path layer-by-layer to produce a 3D object. It generally uses continuous filaments of pure thermoplastics or composite materials as feedstock. The filament is continuously fed into a hot nozzle which moves over a build platform and deposits a thin and tacky bead of extruded material that solidifies upon contact with the substrate layer or the build platform. By following raster paths, solid layers are generated and stacked on top of each other to fabricate the final component.

Components made by the FFF process are prone to various defects due to possible deficiencies in raw material and/or manufacturing process. Large variations in filament diameter, high humidity levels [2], and sub-optimum process parameters, e.g., high nozzle temperature [3, 4], result in creation of trapped porosity and non-optimum flow characteristics in the extruder. Non-destructive evaluation (NDE) methods are suitable choices for detecting and evaluating these defects without damaging the fabricated component or altering its properties. Some NDE methods, such as penetrant testing (PT), eddy current testing (ET), magnetic particle testing (MT), and infrared thermographic testing (TT) are mostly used for detecting surface and subsurface defects. Other NDE methods, such as ultrasonic testing (UT) and radiographic testing (RT) can detect internal defects as well. Each of these two methods has its own advantages and disadvantages, and could be suitable in certain applications. UT has high accuracy and is more sensitive to planar defects, while RT can cover larger areas in one shot and is more suitable for detecting non-planar defects [5].

Ultrasonic testing (UT) is a very capable NDE method that employs ultrasonic wave to test and evaluate various types of materials [6]. In UT, ultrasonic waves are transmitted into a test piece and their interactions with surfaces and internal anomalies are observed. One of the advanced ultrasonic testing techniques is phased array ultrasonic testing (PAUT), in which the ultrasonic probe is made of many piezoelectric crystals laid in a specific patten (linear, circular, annular, or mosaic). Each crystal is excited independently and this makes it possible to generate ultrasonic waves with desired angles and focal points. Angulation and focusing of waves are controlled electronically, and this provides many capabilities for PAUT which are not possible with other UT techniques. Moreover, the recently developed full matrix capture (FMC) and total focusing method (TFM) schemes for collection and interpretation of PAUT data have given PAUT further capabilities in detection and evaluation of defects [7, 8].

Various UT techniques have been used for in-situ and off-line testing of components manufactured by FFF [9]. Koskelo and Flynn [10] carried out in-situ tests on polymeric samples manufactured by FFF process. They attached an ultrasonic probe to the build plate of a FFF 3D printing machine and scanned the sample surface layer by layer using a laser doppler vibrometer. They showed that

inter-layer defects, inclusions, and localized heating damages are easily detectable by this approach. Cummings et al. [11] used an in-situ ultrasonic testing technique for detection of defects in FFF samples. Four piezoelectric crystals were attached to the build plate and excited by a chirp signal every thirty seconds. The resonance frequencies of the sample were then recorded and compared with the data collected from a reference sample. They concluded that online monitoring could be feasible for detection of delamination in FFF 3D printed parts. Na and Oneida [12] used an immersion ultrasonic imaging system, initially developed for visualization of microscopic features in welded metal sheets, for inspection of polymer AM components. This system incorporated 20-MHz focused ultrasonic transducers to test a plastic sample manufactured by FFF process. The test sample was made from ULTEM™ 9085 thermoplastic filament and was 76.2 × 76.2 × 3.3 mm^3 in size. The tests were carried out in both pulse-echo and through-transmission modes. From the images captured from this sample, the authors could identify internal flaws, conditions of outer and inner surfaces, and areas of unexpected process errors. They also suggested a specific sample that included various features such as cavities, holes, and varying wall thicknesses to be used as a standard block for calibration of FFF manufacturing systems. Yap et al. [13] measured the elastic constants of a polycarbonate-acrylonitrile butadiene styrene (PC-ABS) sample manufactured by FFF process. They considered the samples to be orthotropic and measured the longitudinal and shear wave velocities along different directions to find the nine elastic constants of the samples. They also carried out numerical modeling and destructive tests on these samples. Jin et al. [14] used an ultrasonic elastography method to evaluate the mechanical properties of FFF 3D printed components. The results showed the presence of anisotropic dynamic shear modulus and dynamic Young's modulus in the tested components. Lee et al. [15] incorporated air-coupled ultrasonic tests to detect induced defects in cubic samples with different deposition densities manufactured by FFF process. They concluded that air-coupled UT can be used for detection of non-uniform texture and internal defects in FFF components. Although many works have been carried out in testing and characterizing various components manufactured by FFF process, no one has yet examined the internal structure and layup of manufactured FFF components. In all conventional or phased array ultrasonic tests conducted on FFF components, the test frequencies are under 20 MHz, where the wavelengths are not short enough to detect the intricacies of the internal structure of a FFF component. Higher frequencies result in higher attenuation and this could be a major hurdle in implementing high frequency ultrasound for NDE of attenuative materials. Fortunately, there has been attempts to overcome this problem. One such work is recently reported by Rizwan et al. [16] who used pulse compression techniques to alleviate the effects of attenuation in phased array ultrasonic testing of carbon fiber reinforced polymers (CFRP). Higher test frequencies require more sophisticated hardware and higher sampling frequencies as well, and these should be considered when using higher frequencies.

Defects impact surface roughness, dimensional accuracy, and structural performance of 3D printed parts including their tensile properties [17, 18]. Slonov et al. [19] investigated the effect of the raster angle and air gaps on Izod impact strength and tensile properties of 3D printed specimens.

They observed structural defects in the +45°/-45° specimens, which resulted in low impact resistance for unnotched specimens. In addition, introducing the notch did not change the failure mechanism, which remained generally brittle. For +45°/-45° unnotched specimens, reducing the air gap from 0 to -0.025 mm led to a 142% increase in impact strength, while lowering the air gap to -0.054 mm did not improve it further. On the other hand, tensile properties continuously increased with a decrease in air gap. Fayazbakhsh et al. [20] explored the impact of missing materials leading to gaps, on tensile properties of tensile specimens per ASTM D638. They found that gaps which are transverse to the loading direction (90°) had a more severe impact on mechanical properties compared to defects along the loading direction (0°). They obtained 20.5% reduction in tensile strength and 9.6% reduction and modulus for 90° gaps compared to the non-defective baseline specimens. It should be noted that as-manufactured gaps were not characterized since their areas might have changed due to material deposition from the subsequent layers.

In this paper, PAUT technique is utilized for testing FFF tensile specimens made from polylactic acid (PLA). The frequencies used are in the range of 50 MHz and to the best of our knowledge, such high frequencies have never been used in industrial phased array ultrasonic testing in the past. The high resolution available at such high frequencies makes it possible to visualize the internal structure of the FFF 3D printed parts; something that cannot be easily accomplished by any other UT methods. It should also be noted that higher frequency is associated with higher attenuation and the need for more expensive instruments and higher data acquisition rates. In the process of this project, first, dog bone tensile specimens per ASTM D638 are designed and gaps are intentionally induced in them during the manufacturing process. These specimens are then inspected by immersion ultrasonic testing using a Vevo 3100® medical ultrasound system. The ultrasonic testing process can reconstruct the layups of the specimens and capture any defects or inconsistencies that are formed during the 3D printing process. In the next stage, the specimens are dried and subjected to destructive tensile testing to relate their mechanical properties to the as-manufactured gap widths. The paper concludes with main findings from the study and recommends directions for future research.

2. Methodology

2.1. Specimen design and manufacturing

Dog bone tensile specimens per ASTM D638-14 type I are selected for this study [21]. Figure 1 shows dimensions used for the specimen 3D model. The nominal thickness of the specimen is 3.36 mm.

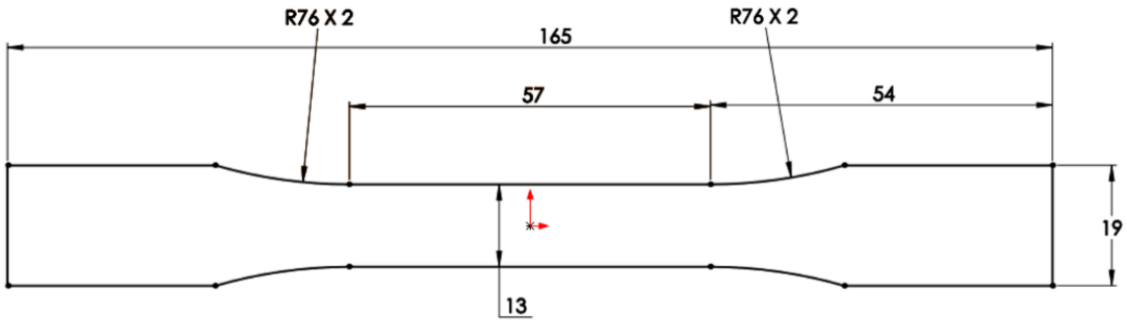

Figure 1. Specimen dimensions per ASTM D638-14 type I, mm.

A quasi-isotropic layup, $[45/0/90/-45]_{3s}$, with a total of 24 layers, each 0.14 mm thick, is chosen for the specimens. A pristine specimen (without any gaps) is considered as the baseline and is called Specimen A. Under-extrusion creates gaps between extrudates (raster) that are in-plane printing issues and can be long throughout part boundaries [22]. Here, gaps are in the form of 5, 7, 8, and 11 adjacent missing extrudates in layer #10 (0° raster angle) for specimens B, C, D, and E, respectively. Gaps are intentionally induced in the center of the specimens and along their length by moving the nozzle head without extruding materials. Figure 2 presents a visualization of layer #10 in specimens A (baseline), B (5 missing extrudates), and E (11 missing extrudates) in Simplify3D version 4.1.2. Figure 2a also shows the nozzle travel moves (red lines) that their significance will be discussed in Section 3.1. It should be noted that gaps with known geometrical dimensions are considered to form a baseline for the validation of the inspection technique.

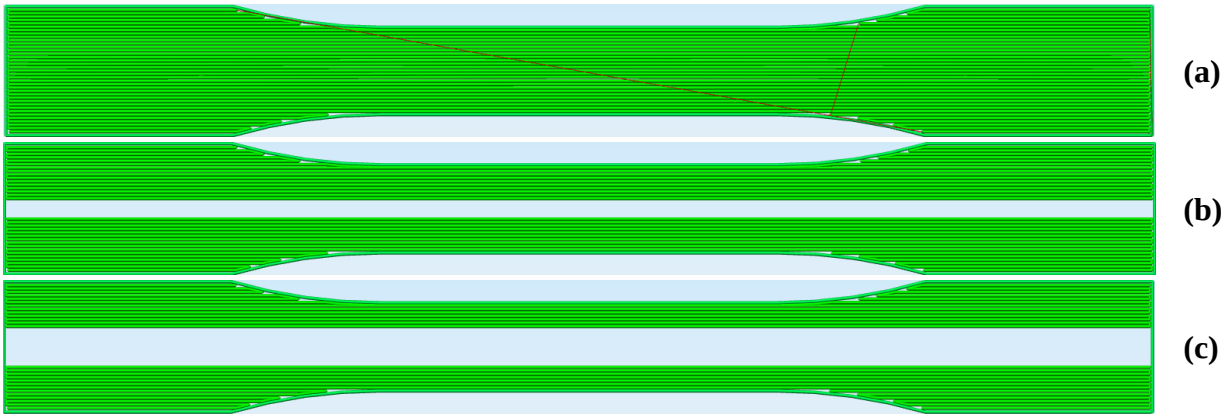

Figure 2. Visualization of layer #10 in dog bone tensile specimens: (a) specimen A; (b) specimen B; and (c) specimen E.

It should be noted that there are 27 extrudates in the narrow section of the baseline, specimen A. Per design, the gap width for defective specimens B, C, D, and E is 2.471, 3.387, 4.333, and 5.308 mm, respectively. It should be recalled that the narrow section and overall widths of the specimen are 13 and 19 mm, respectively (Figure 1). A Prusa i3 Mk2S 3D printer (Prusa Research a.s., Prague, Czechia) firmware version 3.1.0 was used for manufacturing specimens out of PLA from

one batch. Design and manufacturing parameters for 3D printing are summarized in Table 1. Five samples for each set (specimens A to E) were 3D printed for a total of 25 specimens. Laboratory temperature and humidity during 3D printing were between 18 to 21°C and 31.1% to 76.3% relative humidity (RH), respectively.

Table 1. Manufacturing and design parameters for 3D printing.

Manufacturing/design Parameter	Value	Manufacturing/design Parameter	Value
Build orientation	XYZ	Material	PLA
Filament diameter	1.75 mm	Nozzle diameter	0.4 mm
Layer height	0.14 mm	Nozzle temperature	215 °C
Bed platform temperature	60 °C	Cooling	No fan cooling
Printing speed	2400 mm/min	Infill %	100%
Raster angle	$[45/0/90/-45]_{3s}$	Defect inclusion	See Section 2.1

2.2. High frequency phased array ultrasonic testing (PAUT)

The UT system used here is Vevo 3100® (Fujifilm VisualSonics, Toronto, Canada) ultrasound system originally designed for preclinical applications. This system can also be used for industrial applications since the principles of medical ultrasound and industrial ultrasonic testing are the same [16, 23]. The only difference between these two applications is the acoustic impedance of the matching layers used in their probes. In industrial applications, the probes are used for testing high impedance materials such as steel and aluminum but in medical applications, the test material is usually a low-impedance material such as skin or tissue. In this work, the tests are carried out in water and there are no issues with the acoustic matching of the medical probes since the acoustic impedance of water is almost the same as human tissue.

The PAUT probe is a 256-element MX700® probe (Fujifilm VisualSonics, Toronto, Canada) with a center frequency of 50 MHz and a 6-dB bandwidth of 85%. The tests are carried out in immersion mode where both the probe and the sample are immersed in water. The test setup for immersion ultrasonic testing of FFF 3D printed specimens is shown in Figure 3. Both the probe and the UT system were calibrated before conducting the tests. At a frequency of 50 MHz, the depth resolution is 30 microns, and the lateral resolution is 75 microns.

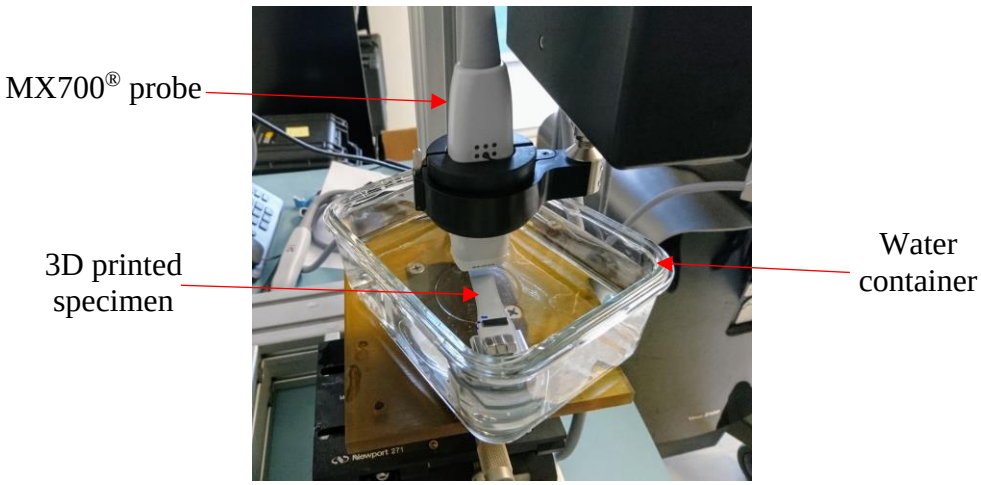

Figure 3. PAUT setup showing a 3D printed specimen and MX700® ultrasonic probe immersed in water.

An area of 64 mm × 8.7 mm in the middle of the specimen is scanned as shown in Figure 4. It should be noted that the maximum gap width for defective samples (specimen E) is 5.31 mm per design; therefore, the scanned width of 8.7 mm is large enough to capture all defects. Gaps are almost uniform along the specimen length (0° raster); therefore, it would suffice if only a portion of the length of a defect is evaluated. The narrow section of the dog bone tensile specimen, where acceptable breakage must occur, is 57 mm (Figure 1). As a result, the scanned length of 64 mm can detect the gaps that impact the tensile properties of the specimens.

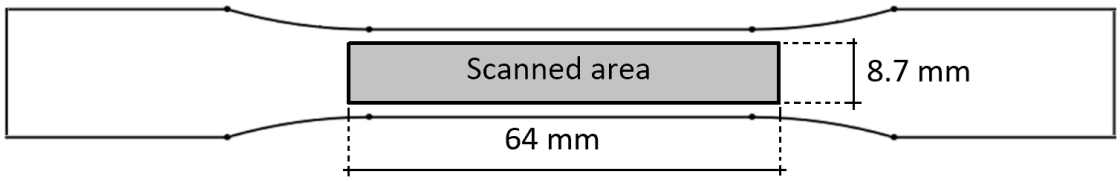

Figure 4. Scanned area of the 3D printed specimens in PAUT.

The 64 mm length along the specimens is scanned using a linear motorized scanner. In the transverse direction, the scanning is performed electronically by the linear phased array probe. The probe sequentially fires several adjacent elements to generate the desired focused ultrasonic wave and then the ultrasonic beam moves along the probe to complete the transverse scan of the specimen. By changing the time delay of the probe elements, the focal point is continuously changed in both transmit and receive stages of the test. This process is called dynamic focusing and greatly enhances the accuracy of measurements [24, 25]. It also provides the depth-wise scanning of the specimens. The electronic scanning and dynamic focusing are performed by computer programs that control the ultrasonic system. Ultrasonic signals are collected every 50 µm during the linear scanning of the sample at a sampling rate of 190 MSamples/s; however, the final image resolution on the screen is much finer due to upsampling process that makes the image fit the screen pixel count.

As mentioned in Section 2.1, five specimens for each gap width were 3D printed and scanned by the PAUT system. After completion of ultrasonic tests, all specimens were placed inside a dehydrator (Noztek, Shoreham, West Sussex, UK) at 40°C overnight to reduce their humidity level caused by water immersion during ultrasonic testing. Finally, specimens were tested per ASTM D638-14 in a United mechanical testing machine with a 10 kN load-cell and an extensometer with 25% strain limit. The speed of testing was 5 mm/min, and the load-extension curve was recorded until rupture for all specimens.

3. Results and discussion

3.1. High frequency phased array ultrasonic testing (PAUT) results

Pristine specimens

Figure 5 shows the 3D scanned image of specimen A-1 where all 24 layers are detected in one single scan. The scanned area is 8.7 mm × 19 mm. The fact that the layers of this specimen are discerned so well means that the ultrasonic waves have reflected from the interfaces of the specimen layers. In other words, there is an impedance mismatch at layer interfaces due to which the ultrasonic wave can be reflected. The high sensitivity of the current technique in distinguishing individual layers could be attributed to the very small wavelength resulting from utilization of the high frequency (50 MHz) probe. The difference between the gray shades of the layers is due to the settings of the probe and can be overcome by optimizing the instrument settings. Currently, the instrument settings are configured for preclinical applications and does not allow us to make much change to them.

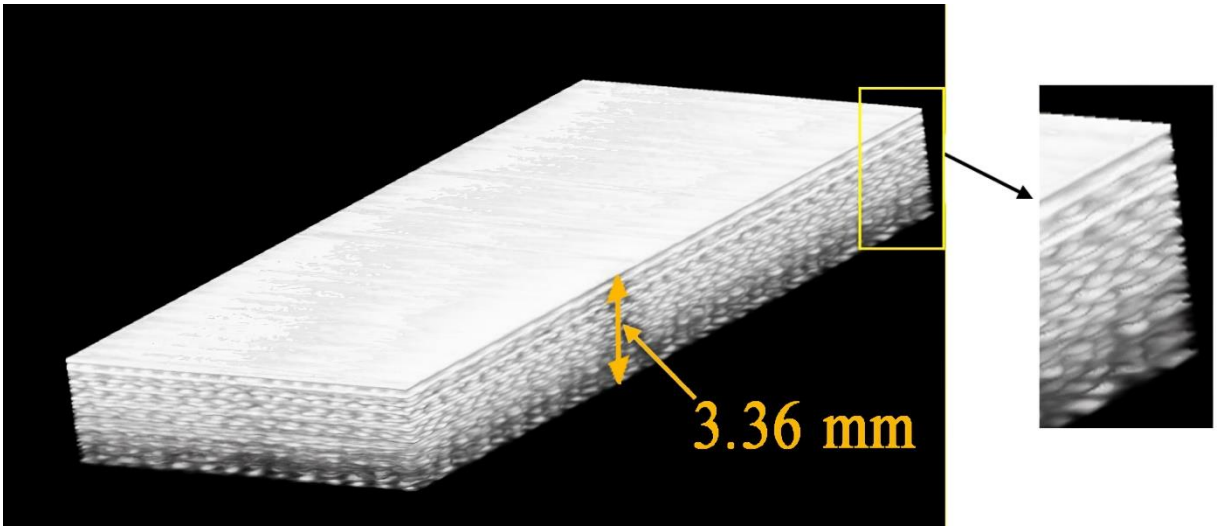

Figure 5. 3D scanned image of specimen A-1, the baseline.

The scanned image is three dimensional, which makes it possible to view the raster angle of each layer one by one. Layers #16 to #19 with raster angles of 45°, -45°, 90°, and 0°, respectively, are

shown in Figure 6. The raster angle for each layer can be clearly observed in the scanned images and agrees with the design. In addition, Figure 6d shows inconsistency during 3D printing of the 0° layer that is due to the nozzle travel moves. It should be recalled that red lines in Figure 2a show the nozzle travel moves while 3D printing a 0° ply. This means that the nozzle does not extrude material but moves along those lines to continue with the 3D printing of the 0° layer. Most of the time, molten material drips while the nozzle moves to its new starting point, which are clearly captured in the scanned area of the specimen for layer #19 with 0° raster angle (Figure 6d). This further confirms that PAUT can be effectively used to capture inconsistencies and defects emerged during 3D printing of a specimen. There are no nozzle travel moves in the scanned area for the other layers and no issues are observed in their corresponding images. It is noteworthy that the image quality is not the same for different layers and not all 24 layers of the sample are discernible as good as the layers shown in Figure 6. The ability to resolve various layers of a specimen depends on the focal point of the transducer. The ultrasonic transducer used in this work has a fix elevation focus at 5 mm. The highest resolution is achieved at the depth where the azimuthal focus, which is driven electronically, meets the elevation focus. As a result, only part of the specimen thickness was captured with the highest resolution.

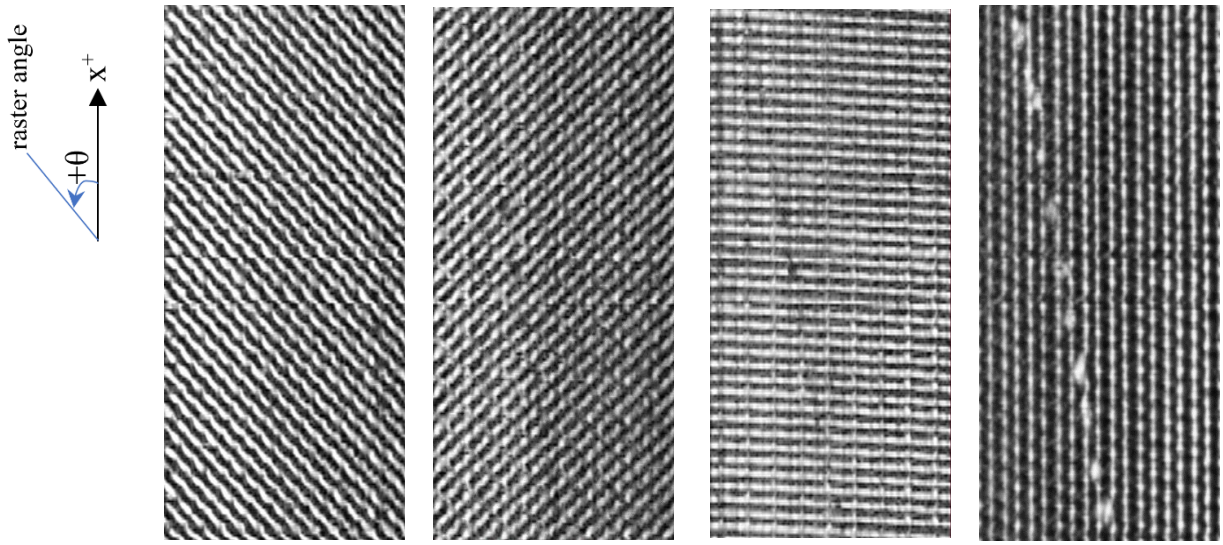

Figure 6. Scanned images of individual layers extracted from the 3D scanned image of specimen A-1 (the baseline): (a) layer #16, 45°; (b) layer #17, -45°; (c) layer #18, 90°; and (d) layer #19, 0°. The scanned area is 8.7 mm × 19 mm.

To demonstrate the capability of the PAUT system in detecting the layup of specimen A-1, a CAD model of a $[45/0/90/-45]_{3s}$ specimen, the same stacking sequence as specimen A, was created. Figure 7a shows a 45-degree cut of this specimen on one of its sides and Figure 7b presents the 3D image of specimen A-1 scanned by PAUT and cut in the same manner. Comparison of Figures 7a and 7b shows that the cross-sections of the CAD drawing and the PAUT image match very well confirming that the PAUT technique can accurately detect the orientation of layers in 3D printed

polymeric parts. In Figure 7b, like Figure 5, the differences in gray shades of the layers do not have any significance as they could be removed by proper setting of the UT instrument. The instrument setting is currently configured for preclinical applications and cannot be changed much. Examination of the layers of a multi-layer specimen is of interest in other applications as well. One such application is detection of stacking sequence in fiber reinforced composites [26, 27]. Nelson and Smith [26] used radon transform to extract the layer stacking sequence and fiber orientation in carbon fiber reinforced composites. Yang et al. [27] incorporated analytic-signal procedure along with log-Gabor filter to improve the quality of the extracted ply parameters in a CFRP specimen. These processing techniuqes can be used in the future to improve the quality of measurements reported in the current research work.

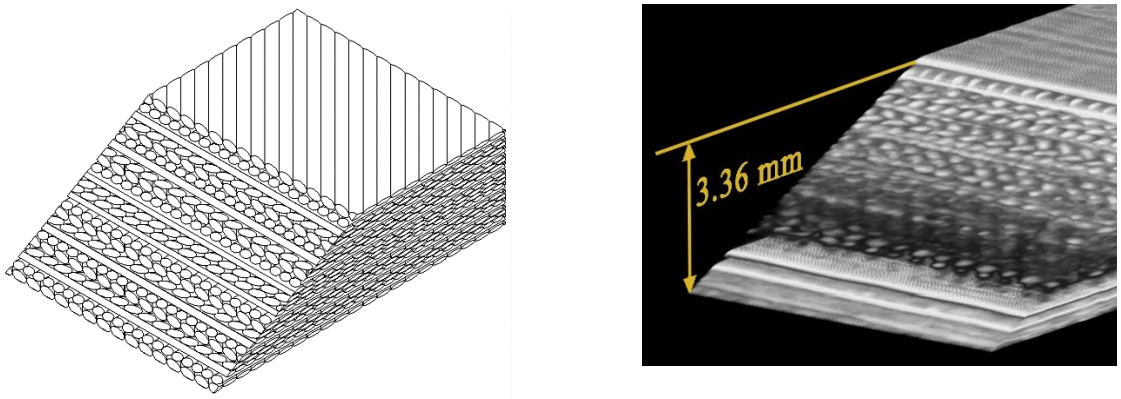

(a) **(b)**

Figure 7. Layup of specimen A-1: (a) CAD drawing; and (b) image obtained by PAUT scanning.

Defective specimens

The output of the ultrasonic system can be displayed as a 3D image in the Fujifilm VisualSonics VevoLab® software. This allows for inspection of the layers of a 3D printed component one by one. Figure 8a shows layer 10 of specimen A-1 (the baseline) which has no gap. Figure 8b shows the same depth for specimen B-2, which includes five missing extrudates. The defect region is clearly distinguishable as a strip with a different gray shade in the middle of specimen B-2.

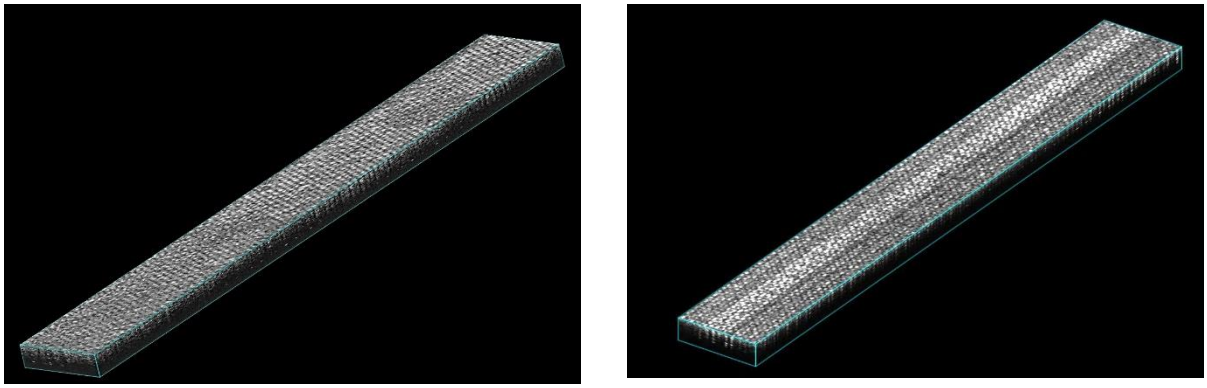

(a) **(b)**

Figure 8. 3D images of tensile specimens at layer #10 obtained by the PAUT technique: (a) specimen A-1 (no gap); and (b) specimen B-2 (with gap). The scanned area is 8.7 mm × 64 mm.

To measure the width of the gap, a 2D representation of layer #10 is used and three measurements are made along the strip (see Figure 9). The process is followed for all defective specimens and the results are reported in Table 2 along with their means and coefficients of variation (CV). CV is the ratio of the standard deviation to the mean and is presented as a percentage. All specimen sets have small CVs (less than 2.30%) except for specimen C, which shows the repeatability of the process. Specimen C-5 has a gap width which is higher than those of specimens C-1 to C-4. Removing specimen C-5, the CV of gap width measurements for specimens C-1 to -4 is only 1.90%. Since the same G-code was used for manufacturing specimens C-1 to C-5, all 3D printing process and design parameters were kept constant. Therefore, the difference in gap width among specimen set C could be due to tolerances in the filament diameter and/or machine errors. It should be noted that the measured defect widths are not dependent on the material from which the samples are manufactured, and only depend on the lateral resolution of the ultrasonic system.

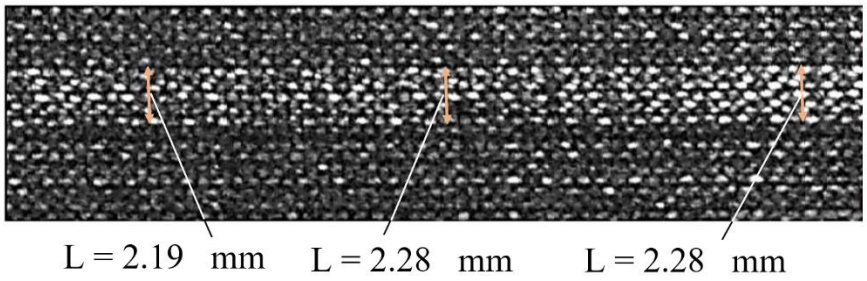

Figure 9. A portion of the scanned image of layer #10 for specimen B-4.

Table 2. Gap widths measured by ultrasonic testing.

Specimen ID	Width 1 (mm)	Width 2 (mm)	Width 3 (mm)	Mean (mm)	Mean (mm)	CV (%)
B-1	2.15	2.28	2.28	2.24		
B-2	2.28	2.29	2.19	2.25		
B-3	2.24	2.24	2.37	2.28	2.25	0.87
B-4	2.28	2.28	2.19	2.25		
B-5	2.24	2.19	2.27	2.23		
C-1	2.94	2.85	2.94	2.91		
C-2	2.98	2.94	3.07	3.00		
C-3	2.94	2.98	2.94	2.95	3.05	7.81
C-4	2.90	2.98	2.89	2.92		
C-5	3.38	3.58	3.47	3.47		
D-1	4.57	4.57	4.52	4.55		
D-2	4.39	4.39	4.47	4.41		
D-3	4.56	4.61	4.61	4.59	4.50	2.30
D-4	4.43	4.39	4.30	4.37		
D-5	4.52	4.65	4.61	4.59		

E-1	5.00	5.04	4.91	4.98	5.04	1.09
E-2	5.05	5.09	5.00	5.05		
E-3	5.08	4.95	5.13	5.05		
E-4	5.00	4.96	5.00	4.98		
E-5	5.13	5.17	5.05	5.11		

Table 3 compares the as-designed gap width from Simplify3D and as-manufactured gap width measured by PAUT system for different specimen sets. Assuming the gap width from the Simplify3D as the base for comparison, the error percentages in the measured values was calculated. The error is below 10% and the measured gap width is smaller (except for specimen set D) than the as-designed value. This is expected since when layers subsequent to layer #10 (0° layer with a gap) are deposited, they push on the extrudates in layer #10 and force materials to the gap area, resulting in a smaller gap width. If the magnitude of the errors is considered, specimen set D has the lowest value, which means a close match between as-designed gap width from Simplify3D and as-manufactured gap width measured by the PAUT system. Tolerances in the filament diameter and/or machine errors could have contributed to this difference among specimen sets, which requires further investigation.

Table 3. Gap width for different specimen sets.

Specimen ID	No. of missing extrudates	As designed mean gap width (mm)	As manufactured mean gap width (mm)	Error (%)
Specimen B	5	2.471	2.25	-8.9%
Specimen C	7	3.387	3.05	-9.9%
Specimen D	9	4.333	4.50	3.8%
Specimen E	11	5.308	5.04	-5.1%

Tensile properties of 3D printed specimens are impacted by gaps and they can be used as an indication of the gap width. Section 3.2 presents tensile testing results of the specimens after ultrasonic testing and a subsequent drying process to bring them to the standard laboratory environment.

3.2. Tensile testing results

Five tensile samples for each specimen set (a total of 25) were tested until failure and their Young's moduli, tensile strengths, and failure strains were obtained. The maximum normed residual (MNR) method was used to screen all tensile properties for outliers [28]. All specimens had lower MNR values (a maximum of 1.632 for specimen A-2) than the critical value of 1.715 for the sample size of five. Therefore, all testing results were used in the statistical analysis to find mean and CV for all the specimen sets. Table 4 summarizes tensile properties of the specimen sets considering their as-manufactured mean gap width obtained from the PAUT technique.

Table 4. Tensile properties of the five specimen sets.

Specimen ID	Gap width (mm)	Young's modulus		Tensile strength		Failure strain	
		Mean (GPa)	CV	Mean (MPa)	CV	Mean (%)	CV
Specimen A	0	2.85	1.14%	42.4	1.44%	2.81	19.6%
Specimen B	2.25	2.83	2.17%	41.8	0.76%	2.57	6.5%
Specimen C	3.05	2.76	2.65%	40.4	0.63%	2.73	14.8%
Specimen D	4.50	2.75	0.87%	41.1	0.80%	2.74	17.6%
Specimen E	5.04	2.70	1.60%	40.4	1.40%	2.56	24.3%

As seen in Table 4, the CV for Young's modulus and tensile strength is below 3%, which confirms that the results can be used for comparing different specimen sets. On the other hand, failure strain has the highest CV (a maximum of 24.3%), which seems to be the case in testing polymeric 3D printed specimens per ASTM D638 and was observed by the authors in an earlier work [20]. With an increase in the as-manufactured gap width, there is a decrease in Young's modulus from 2.85 to 2.70 GPa for the baseline and the widest gap, 5.036 mm, respectively. The same trend is also observed for tensile strength, where there is almost a continuous decrease in its values with an increase in the gap width except for Specimen D. The baseline (no gap) has a tensile strength of 42.4 MPa, while Specimen set E (maximum gap width) has the lowest tensile strength of 40.4 MPa among all samples. Gaps are missing extrudates and materials in a specimen and they are expected to reduce Young's modulus and tensile strength of the specimens [20]. This trend was observed for the specimen sets investigated here and validates the gap width values obtained by the PAUT technique.

4. Conclusions

High frequency phase array ultrasonic testing (PAUT) was used as a non-destructive evaluation (NDE) technique to locate defects in polymeric 3D printed parts. Gaps were intentionally induced in dog bone tensile specimens as missing extrudates in a layer with 0° raster angle. A total of 25 specimens were 3D printed from PLA with different gap widths including a baseline (pristine specimen set). A Vevo 3100® ultrasonic system with an MX700® probe were used for immersion ultrasonic testing of the manufactured specimens. High-resolution images from individual layers of a pristine specimen were captured in one single scan, and clearly showed the raster angles, which agreed with the design. In addition, unwanted molten filament dripping from the nozzle was captured as a 3D printing inconsistency. For defective specimens, the defect region was distinguishable in the images obtained from the ultrasonic system, and the widths of the missing extrudates were measured. The measured gap width was generally smaller than the as-designed value with an error below 10%. Tensile testing on all specimens was performed until rupture as an indication of the gap width. The pristine specimens (no gap) had the highest tensile modulus and strength among all specimens (2.85 GPa and 42.4 MPa), while specimens with maximum gap width had the lowest values (2.70 GPa and 40.4 MPa).

In this study, gaps were examined as one of the possible defects induced by FFF 3D printing machines. Other types of defects, e.g., voids and overlaps, can also be investigated. In addition, the PAUT technique can be used in 3D printed parts after annealing to evaluate defects variation due to this post-processing method. PAUT results can be improved by modifying the focusing techniques so that the whole thickness of a specimen can be examined with high resolution. Investigating the effects of various PAUT parameters on the final product and performing tests on FFF 3D printed parts from different thermoplastic materials can also be explored in the future. It should be noted that polymeric materials are highly attenuative and inspection of thick components might be challenging.

Acknowledgements
Authors wish to acknowledge the financial support of Natural Sciences and Engineering Research Council (NSERC) of Canada, Engage Program (Grant No. 1-51-47218) through A. Varvani of Ryerson University and A. Needles of FUJIFILM VisualSonics. Authors also acknowledge the Natural Sciences and Engineering Research Council of Canada (NSERC, RGPIN-2018-04144).

References
[1] "ISO/ASTM, E. 52900. Additive manufacturing—General principles—Terminology," ed: International Organization for Standardization: Geneva, Switzerland. 2015.
[2] Zaldivar, R.J., Mclouth, T.D., Ferrelli, G.L., Patel, D.N., Hopkins, A.R. and Witkin, D., 2018. Effect of initial filament moisture content on the microstructure and mechanical performance of ULTEM® 9085 3D printed parts. Additive Manufacturing, 24, pp.457-466.
[3] Kuznetsov, V.E., Solonin, A.N., Tavitov, A., Urzhumtsev, O. and Vakulik, A., 2020. Increasing strength of FFF three-dimensional printed parts by influencing on temperature-related parameters of the process. Rapid Prototyping Journal.
[4] Foppiano, M., Saluja, A., Fayazbakhsh, K., Experimental study on interlayer tensile strength and temperature history of 3D printed specimens, Submitted to the Virtual and Physical Prototyping journal.
[5] P. J. Shull, Nondestructive Evaluation: Theory, Techniques, and Applications. Marcel Dekker, 2002.
[6] A. B. Lopez, J. Santos, J. P. Sousa, T. G. Santos, and L. Quintino, "Phased Array Ultrasonic Inspection of Metal Additive Manufacturing Parts," Journal of Nondestructive Evaluation, vol. 38, no. 3, p. 62, 2019.
[7] C. Holmes, B. W. Drinkwater, and P. D. Wilcox, "Post-processing of the full matrix of ultrasonic transmit–receive array data for non-destructive evaluation," NDT & e International, vol. 38, no. 8, pp. 701-711, 2005.
[8] C. Holmes, B. W. Drinkwater, and P. D. Wilcox, "Advanced post-processing for scanned ultrasonic arrays: Application to defect detection and classification in non-destructive evaluation," Ultrasonics, vol. 48, no. 6-7, pp. 636-642, 2008.

[9] Honarvar, F. and Varvani-Farahani, A., 2020. A review of ultrasonic testing applications in additive manufacturing: Defect evaluation, material characterization, and process control. Ultrasonics, Vol. 108, 106227. DOI: 10.1016/j.ultras.2020.106227
[10] E. C. Koskelo and E. B. Flynn, "Scanning laser ultrasound and wavenumber spectroscopy for in-process inspection of additively manufactured parts," in Nondestructive Characterization and Monitoring of Advanced Materials, Aerospace, and Civil Infrastructure 2016, 2016, vol. 9804: International Society for Optics and Photonics, p. 980418.
[11] I. Cummings, E. Hillstrom, R. Newton, E. Flynn, and A. Wachtor, "In-process ultrasonic inspection of additive manufactured parts," in Topics in Modal Analysis & Testing, Volume 10: Springer, 2016, pp. 235-247.
[12] J. K. Na and E. K. Oneida, "Nondestructive evaluation method for standardization of fused filament fabrication based additive manufacturing," Additive Manufacturing, Article vol. 24, pp. 154-165, 2018, doi: 10.1016/j.addma.2018.09.024.
[13] Yap, Y.L., Toh, W., Koneru, R., Lin, K., Yeoh, K.M., Lim, C.M., Lee, J.S., Plemping, N.A., Lin, R., Ng, T.Y. and Chan, K.I., 2019. A non-destructive experimental-cum-numerical methodology for the characterization of 3D-printed materials—polycarbonate-acrylonitrile butadiene styrene (PC-ABS). Mechanics of Materials, 132, pp.121-133.
[14] Jin, Y., Yang, T., Heo, H., Krokhin, A., Shi, S.Q., Dahotre, N., Choi, T.Y. and Neogi, A., 2020. Novel 2D dynamic elasticity maps for inspection of anisotropic properties in fused deposition modeling objects. Polymers, 12(9), p.1966.
[15] Lee, J., Hasanian, M., Saboonchi, H., Baechle, M. and Taheri, H., 2020, April. Ultrasonic evaluation of polymer additively manufactured parts for defect inspection and structural integrity assessment. In Nondestructive Characterization and Monitoring of Advanced Materials, Aerospace, Civil Infrastructure, and Transportation XIV (Vol. 11380, p. 113801Q). International Society for Optics and Photonics.
[16] M. K. Rizwan, S. Laureti, H. Mooshofer, M. Goldammer, and M. Ricci, "Ultrasonic Imaging of Thick Carbon Fiber Reinforced Polymers through Pulse-Compression-Based Phased Array," *Applied Sciences*, vol. 11, no. 4, p. 1508, 2021.
[17] Wickramasinghe, S., Do, T. and Tran, P., 2020. FDM-based 3D printing of polymer and associated composite: A review on mechanical properties, defects and treatments. Polymers, 12(7), p.1529.
[18] Ngo, T.D., Kashani, A., Imbalzano, G., Nguyen, K.T. and Hui, D., 2018. Additive manufacturing (3D printing): A review of materials, methods, applications and challenges. Composites Part B: Engineering, 143, pp.172-196.
[19] Slonov, A.L., Khashirov, A.A., Zhansitov, A.A., Rzhevskaya, E.V. and Khashirova, S.Y., 2018. The influence of the 3D-printing technology on the physical and mechanical properties of polyphenylene sulfone. Rapid Prototyping Journal.
[20] Fayazbakhsh, K., Movahedi, M. and Kalman, J., 2019. The impact of defects on tensile properties of 3D printed parts manufactured by fused filament fabrication. Materials Today Communications, 18, pp.140-148.

[21] ASTM D638-14, 2014. ASTM International. Standard test method for tensile properties of plastics.
[22] Jin, Z., Zhang, Z. and Gu, G.X., 2019. Autonomous in-situ correction of fused deposition modeling printers using computer vision and deep learning. Manufacturing Letters, 22, pp.11-15.
[23] P. Payne, "Medical and industrial applications of high resolution ultrasound," Journal of Physics E: Scientific Instruments, vol. 18, no. 6, p. 465, 1985.
[24] L. W. Schmerr Jr, Fundamentals of ultrasonic phased arrays. Springer, 2014.
[25] L. Chen, W. Wei, J. Yongliang, W. Chenghao, Z. Qingxi, and P. Yunxuan, "Ultrasonic digital phased array dynamic focusing system," Appl. Acoust, vol. 19, pp. 14-18, 2000.
[26] L. Nelson and R. Smith, "Fibre direction and stacking sequence measurement in carbon fibre composites using Radon transforms of ultrasonic data," Composites Part A: Applied Science and Manufacturing, vol. 118, pp. 1-8, 2019.
[27] X. Yang, E. Verboven, B.-f. Ju, and M. Kersemans, "Parametric study on interply tracking in multilayer composites by analytic-signal technology," Ultrasonics, vol. 111, p. 106315, 2021.
[28] MIL-HDBK-17F (2002) Composite material handbook, Polymer matrix composite guidelines, vol. 1.